

FRACTURE ANALYSIS IN AN ORTHOTROPIC ROTATING HYPERBOLIC DISC FITTED WITH STIFF ROD


ANALIZA LOMA ORTOTROPNOG ROTIRAJUĆEG HIPERBOLIČKOG DISKA SA KRUTIM ŠTAPOM


Originalni naučni rad / Original scientific paper

Rad primljen / Paper received: 26.06.2024

<https://doi.org/10.69644/ivk-2024-03-0339>

Adresa autora / Author's address:

¹⁾ Jaypee Institute of Information Technology, A-10, Sector 62, Noida (Uttar Pradesh), India Pin code 201307 R. Sharma  0009-0007-2895-9626 *email: richa.ggit@gmail.com

²⁾ University of Belgrade, Faculty of Mechanical Engineering, Belgrade, Serbia Z. Radaković  0000-0001-8054-470X

Keywords

- orthotropic material
- hyperbolic disc
- rotating disc
- fracture
- transition theory

Abstract

The main objective of the problem is to evaluate the stresses and displacement in an orthotropic hyperbolic spinning disc equipped with a stiff rod that has a changeable density parameter. The methodology of transition theory developed by B.R. Seth is applied to simplify the governing differential equation of the considered physical problem. This theory has the advantage of taking the material's non-linear character into account. Based on the stress analysis of rotating discs composed of various orthotropic materials, the following conclusions are reached: the angular velocity is maximal in the convergent disc made of topaz material (orthotropic) in elastic state, but in the plastic state angular velocity is maximal for divergent disc of steel. When compared to other materials under consideration, the diverging disc constructed of barite has the largest stresses in the elastic state and compressive fully plastic stresses are the highest in the diverging disc of topaz at the outer surface. Based on all numerical calculations and graphs it is observed that the convergent disc of topaz is a better option for the designing purpose compared to the other materials.

INTRODUCTION

Many studies have been conducted to analyse the deformations, failure and stresses in a spinning disc with hyperbolic behaviour under various situations such as high temperature and pressure, etc. Due to their significance in numerous engineering applications in aerospace industries, mechanical components such as compressors, turbo generators, flywheels, sink fits, high speed gear engines, pumps, steam turbines, computer discs, etc., elasto-plastic rotating discs have consistently sparked a lot of research. The evaluated disc is fitted with a shaft.

Analytical investigations of elasto-plastic rotating discs can be found in /1-5/. Sharifi /6/ employed the Lord-Shulman coupled theory of thermoelasticity to analytically solve the issue of thermal shock in an orthotropic rotating disc. The plastic deformation of a revolving disc constructed of aluminium dispersion-hardened alloys was researched using mechanical tensile tests and structural investigation utilis-

Ključne reči

- ortotropni materijal
- hiperbolički disk
- rotirajući disk
- lom
- teorija prelaznih napona

Izvod

Osnovna svrha zadatog problema sastoji se u proračunu napona i pomeranja ortotropnog hiperboličkog rotirajućeg diska sa krutim štapom, promenljivog parametra gustine. Primljena je metodologija prelaznih napona, koju je razvio B.R. Seth, radi pojednostavljenja date polazne diferencijalne jednačine zadatog fizičkog problema. Prednost ove teorije je uzimanje u razmatranje nelinearnih karakteristika materijala. Na osnovu naponske analize rotirajućih diskova sačinjenih od raznih ortotropnih materijala, dolazi se do sledećih zaključaka: ugaona brzina je maksimalna u konvergentnom disku od materijala topaza (ortotropan) u elastičnom stanju, dok je ugaona brzina u plastičnom stanju maksimalna kod divergentnog diska od čelika. Poređenjem ostalih razmatranih materijala, kod divergentnog diska od barita se javlja najveći naponi u elastičnom stanju, a pritisni potpuno plastični naponi su najveći kod divergentnog diska od topaza na spoljnoj površini. Na osnovu svih numeričkih proračuna i grafičkih prikaza uočava se da je konvergentni disk od topaza pogodnija opcija u projektovanju u odnosu na ostale materijale.

ing optical microscope techniques by Matvienko and others /7/. Bayat and Nazari /8/ employed the extended finite element method (XFEM) to investigate a cracked orthotropic medium under a non-classic thermal shock considering the Green-Naghdi (GN) theory of thermoelasticity (type II). Zanchini and others /9/ discuss the design of a composite and an aluminium spoke-type wheels and performed FE and experiments for cornering and radial fatigue on the wheels. Thakur and Verma /10/ employed Seth's transition theory for the evaluation of creep stresses in the spherical shell composed of different materials subjected to uniform internal pressure. Godana et al. /11/ calculated creep transition stresses and strain rates in a spherical shell of isotropic or transversely isotropic materials under a uniform pressure and temperature gradient by applying the Seth transition theory and the extended strain measure theory. Thakur et al. /12/ presented a transition theory-based investigation of the thermal effect in a rectangular plate consisting of rubber, copper, and glass components.

Salehian et al. /13/ employed Galerkin's approach to calculate shear stress and tangential displacement of a rotating disc with varying thickness. Singh et al. /14/ employed threshold stress-based law to evaluate creep stress in rotating composite discs having equal volume with the same average thickness and found that the most effective creep response is provided by a disc with a hyperbolic thickness profile. Lin /15/ investigated the mechanical behaviour on displacement and stress in FGM annular disc subjected to different pressure on internal and external surfaces. Jalali et al. /16/ used finite difference approach to investigate the graded index effect, angular speed, and variable thickness parameters on stresses and deformation. Furthermore, Yildirim /17/ examined the thermomechanical behaviour of a conventionally constructed hyperbolic spinning disc with divergent and convergent profiles. R. Sharma /18/ has found that a disc built of barium titanate (BaTiO_3) performs better than one composed of PZT4 (piezoceramic). Matvienko et al. /19/ studied the plastic deformation of a rotating annular disc formed of aluminium dispersion-hardened alloys using mechanical tensile tests and a structured study using optical microscopy methods. Es-Saheb and Fouad /20/ studied the creep behaviour in a rotating thick-walled cylinder made of Al-SiC_p composite subjected to constant load as well as internal and external pressure, both analytically and numerically, using FEM. Thakur et al. /21/ evaluated the stresses and displacement in hyperbolic rotating disc constructed of isotropic material and found that as compared to aluminium alloy material, the rubber-based convergent disc requires the highest radial stress.

MATHEMATICAL FORMATION OF THE PROBLEM

Assuming symmetry with regard to the mid-plane, let us examine an annular thin disc composed of orthotropic material with inner radius r_1 and outer radius r_2 . The profile of the hyperbolic disc is given in hyperbolic form as

$$h = h_0 \left(\frac{r}{r_1} \right)^k,$$

where: k is the thickness parameter, $k > 0$ (i.e., divergent disc), $k = 0$ (i.e., uniform disc), and $k < 0$ (i.e., convergent disc), respectively depicted in Fig. 1a to 1c. In these cases, the hyperbolic disc rotates along a rod at an angular speed ω that gradually increases in magnitude around an axis. Variable density of the rod is assumed to be $\rho = \rho_0(r/r_2)^t$, where t is the density parameter.

In polar form, the displacement co-ordinates u, v, w are presumed to be

$$u = r(1 - \beta), \quad v = 0, \quad \text{and} \quad w = \alpha z, \quad (1)$$

where: β is a function of $r = \sqrt{(x^2 + y^2)}$; and α is a constant.

The following equations provide the strain components expressed in terms of displacement,

$$e_{rr} = \frac{1}{n} \{1 - [2(r\beta' + \beta) - 1]^{n/2}\}, \quad e_{\theta\theta} = \frac{1}{n} [1 - (2\beta - 1)^{n/2}],$$

$$e_{zz} = \frac{1}{n} [1 - (1 - 2\alpha)^{n/2}], \quad e_{r\theta} = e_{\theta z} = e_{rz} = 0, \quad (2)$$

where: n is the strain measure; and $\beta' = d\beta/dr$.

Hooke's law for orthotropic materials is

$$T_{rr} = C_{11}e_{rr} + C_{12}e_{\theta\theta} + C_{13}e_{zz},$$

$$T_{\theta\theta} = C_{21}e_{rr} + C_{22}e_{\theta\theta} + C_{23}e_{zz},$$

$$T_{zz} = T_{zr} = T_{r\theta} = T_{\theta z} = 0. \quad (3)$$

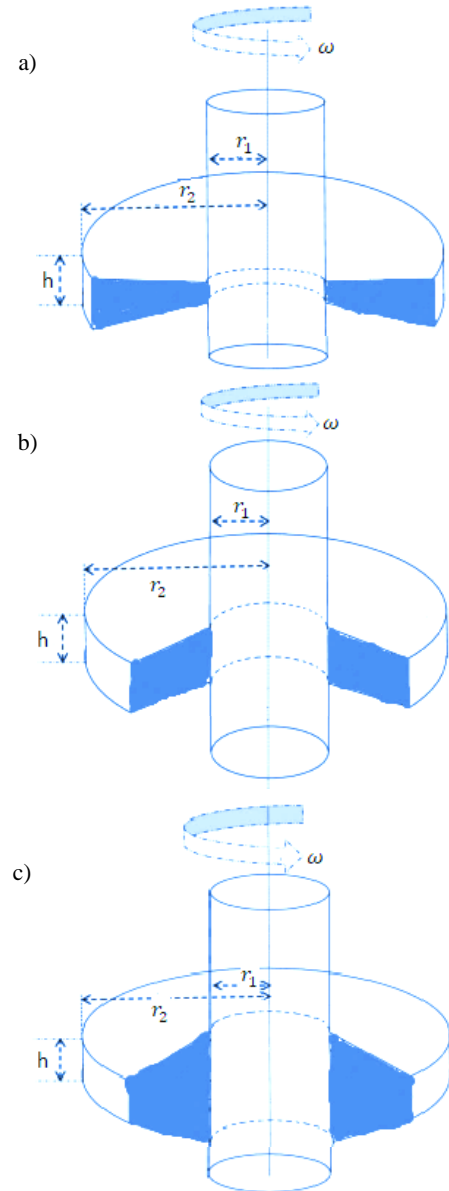


Figure 1. Geometrical representation of hyperbolic rotating disc: a) divergent ($k > 0$); b) uniform ($k = 0$); c) convergent ($k < 0$).

Using Eqs. (2) and (3), stresses are obtained as

$$T_{rr} = \frac{C_{11}}{n} \left[1 - \{2(r\beta' + \beta) - 1\}^{n/2} \right] + \frac{C_{12}}{n} \left[1 - (2\beta - 1)^{n/2} \right] + \frac{C_{13}}{n} \left[1 - (1 - 2\alpha)^{n/2} \right]$$

$$T_{\theta\theta} = \frac{C_{21}}{n} \left[1 - \{2(r\beta' + \beta) - 1\}^{n/2} \right] + \frac{C_{22}}{n} \left[1 - (2\beta - 1)^{n/2} \right] + \frac{C_{23}}{n} \left[1 - (1 - 2\alpha)^{n/2} \right]$$

$$T_{zz} = T_{zr} = T_{r\theta} = T_{\theta z} = 0, \quad (4)$$

where: $r\beta' = \beta P$; C_{11} , C_{12} , C_{13} , C_{21} , C_{22} , and C_{23} are material constants.

The strain components in terms of displacement and stresses for a plane stress case are

$$e_{rr} \equiv \frac{\partial u}{\partial r} = \frac{1}{E_r} T_{rr} - \frac{\nu_{r\theta}}{E_r} T_{\theta\theta}, \quad e_{\theta\theta} \equiv \frac{u}{r} = \frac{1}{E_\theta} T_{\theta\theta} - \frac{\nu_{r\theta}}{E_\theta} T_{rr},$$

$$e_{r\theta} = e_{\theta z} = e_{rz} = 0. \quad (5)$$

The rotating disc's equation of equilibrium: $\frac{d}{dr}(rT_{rr}) - hT_{\theta\theta} + \rho\omega^2 r^2 h = 0$. (6)

Putting values of T_{rr} and $T_{\theta\theta}$ from Eq.(4) in Eq.(6), the following nonlinear differential equation is
$$\left[\beta^2 PC_{11} \{2\beta(P+1)\}^{n/2-1} \right] \frac{dP}{d\beta} = -C_{11}P(P+1)\{2\beta(P+1)-1\}^{n/2-1} - C_{12}\beta P\{2\beta-1\}^{n/2-1} + \frac{C_{11}-C_{21}}{n} [1-\{2\beta(P+1)-1\}^{n/2}] + \frac{C_{12}-C_{22}}{n} \times$$

$$\times [1-\{2\beta-1\}^{n/2}] + \frac{C_{13}-C_{23}}{n} [1-(1-2\alpha)^{n/2}] - \frac{h'r}{h} \left\{ \frac{C_{22}}{n} [1-\{2\beta(P+1)-1\}^{n/2}] + \frac{C_{22}}{n} [1-\{2\beta-1\}^{n/2}] + \frac{C_{23}}{n} [1-(1-2\alpha)^{n/2}] \right\} + \rho_0 \left(\frac{r}{r_2} \right)^t. \quad (7)$$

Boundary conditions are taken as $u = 0$ at $r = r_1$ and $T_{rr} = 0$ at $r = r_2$. (8)

For elastic to plastic transition the transition function is assumed to be

$$\Phi = \frac{C_{11}}{C_{12}} T_{\theta\theta} = \frac{C_{11}}{C_{21}} \left(\frac{C_{21}}{n} [1-\{2(r\beta'+\beta)-1\}^{n/2}] + \frac{C_{22}}{n} [1-(2\beta-1)^{n/2}] + \frac{C_{23}}{n} [1-(1-2\alpha)^{n/2}] \right). \quad (9)$$

Taking logarithmic differentiation of the above Eq.(9) we get

$$\frac{d}{dr} \log \Phi = \frac{C_{11} \left[-\{2(r\beta'+\beta)-1\}^{\frac{n}{2}-1} (P+1) \frac{\beta P}{r} + \frac{\beta P^2}{r} \frac{dP}{d\beta} \right] + \frac{C_{11}C_{22}}{C_{21}} \left[-(2\beta-1)^{\frac{n}{2}-1} \right] \frac{\beta P}{r}}{\frac{C_{11}}{C_{21}} \left(\frac{C_{21}}{n} [1-\{2(r\beta'+\beta)-1\}^{n/2}] + \frac{C_{22}}{n} [1-(2\beta-1)^{n/2}] + \frac{C_{23}}{n} [1-(1-2\alpha)^{n/2}] \right)}. \quad (10)$$

Substituting the value of $dP/d\beta$ from Eq.(7) in Eq.(10) and taking asymptotic value as $P \rightarrow \pm\infty$, we get

$$\frac{d}{dr} \log \Phi = \frac{C-1}{r} + \frac{Ch'}{h}, \quad (11)$$

where: $C = C_{21}/C_{11}$.

On integrating Eq.(10) yields $\Phi = A_1 h^C r^{C-1}$, (12)

where: $C = C_{21}/C_{11}$; and A_1 is constant of integration.

Stresses in terms of transition function $T_{\theta\theta} = CA_1 h^C r^{C-1}$, $T_{rr} = \frac{CA_1 h_0^C r^{Ck+C-1}}{r_1^{Ck}(Ck+C+k)} - \frac{\rho_0 \omega^2 r^{t+2}}{r_2^t(t+k+3)} + \frac{A_2}{rh}$. (13)

Using the stress relations, the displacement is given by

$$u = r \left[\frac{1}{E_\theta} T_{\theta\theta} - \frac{\nu_{r\theta}}{E_\theta} T_{rr} \right], \quad u = r \left[\frac{1}{E_\theta} CA_1 h^C r^{C-1} - \frac{\nu_{r\theta}}{E_\theta} \left\{ \frac{CA_1 h_0^C r^{Ck+C-1}}{r_1^{Ck}(Ck+C+k)} - \frac{\rho_0 \omega^2 r^{t+2}}{r_2^t(t+k+3)} + \frac{A_2}{rh} \right\} \right]. \quad (14)$$

Using boundary conditions from Eq.(8) in Eqs. (13) and (14) we have

$$A_1 = \frac{\rho_0 \omega^2 r_1^{Ck+C} (Ck+C+k)(r_2^{t+k+3} + r_1^{t+k+1}) E_\theta \nu_{r\theta}}{Ch_0^C [r_1^{Ck+C+k} (E_\theta \nu_{r\theta} - E_\theta) + r_2^{Ck+C+k}]}, \quad A_2 = \frac{h_0 \rho_0 \omega^2 r_2^{k+3}}{r_1^k(t+k+3)} - \frac{\rho_0 \omega^2 h_0 r_2^{Ck+C+k} (r_2^{t+k+3} + r_1^{t+k+1}) E_\theta \nu_{r\theta}}{r_1^{Ck+C+k} (E_\theta \nu_{r\theta} - E_\theta) + r_2^{Ck+C+k}}. \quad (15)$$

According to Tresca's yield criterion the initial yielding in the material is assumed to occur at $r = r_1$ (inner surface),

$$|T_{rr} - T_{\theta\theta}|_{r=r_1} = Y, \quad Y = \left| \frac{\rho_0 \omega^2 [r_1^{Ck+C+k-1} - r_2^{Ck+C+k} r_1^{-k-1} - (Ck+C+k) r_1^{C-1} (r_2^{t+k+3} + r_1^{t+k+1}) E_\theta \nu_{r\theta} - \frac{\rho_0 \omega^2 r_1^{t+2}}{r_2^t(t+k+3)} + \frac{\rho_0 \omega^2 r_2^{k+3}}{r_1^{2k+1}(t+k+3)}]}{r_1^{Ck+C+k} (E_\theta \nu_{r\theta} - E_\theta) + r_2^{Ck+C+k}} \right| \quad (16)$$

The value of angular velocity from Eq.(16) is obtained as: $\frac{\rho_0 \omega^2 r_2^2}{Y} =$

$$= \left| \frac{[r_1^{Ck+C+k} (E_\theta \nu_{r\theta} - E_\theta) + r_2^{Ck+C+k}] r_2^t 2^{k+1} (t+k+3)}{[r_1^{Ck+C+k-1} - r_2^{Ck+C+k} r_1^{-k-1} - (Ck+C+k) r_1^{C-1} (r_2^{t+k+3} + r_1^{t+k+1}) E_\theta \nu_{r\theta} r_2^t 2^{k+1} (t+k+3) + (r_2^{k+1} - r_1^{t+1}) [r_1^{Ck+C+k} (E_\theta \nu_{r\theta} - E_\theta) + r_2^{Ck+C+k}]} \right|. \quad (17)$$

For converting all the parameters in non-dimensional form, it is assumed as

$$R = \frac{r}{r_2}, \quad R_0 = \frac{r_1}{r_2}, \quad \sigma_{r1} = \frac{T_{rr}}{Y_1}, \quad \sigma_{\theta 1} = \frac{T_{\theta\theta}}{Y_1}, \quad \sigma_{r2} = \frac{T_{rr}}{Y_2}, \quad \sigma_{\theta 2} = \frac{T_{\theta\theta}}{Y_2}, \quad \Omega_i = \frac{\rho_0 \omega^2 r_2^2}{Y}. \quad (18)$$

Transitional stresses, angular velocity, and displacement in non-dimensional form are: $\frac{\rho_0 \omega^2 r_2^2}{Y} = \Omega_i =$

$$= \left| \frac{[R_0^{Ck+C+k} (E_\theta \nu_{r\theta} - E_\theta) + 1] R_0^{2k+1} (t+k+3) r_2^{Ck+C+3k+3t+4}}{[R_0^{Ck+C+k-1} r_2^{-1} - R_0^{-k-1} r_2^{-k-1} - (Ck+C+k) R_0^{C-1} r_2^{C-1} (1 + R_0^{t+k+1} r_2^{-2}) E_\theta \nu_{r\theta} r_2^{t+2k+1} R_0^{2k+1} (t+k+3) + (r_2^{k+1} - R_0^{t+1} r_2^{t+1}) [R_0^{Ck+C+k} (E_\theta \nu_{r\theta} - E_\theta) + 1]} \right|,$$

$$\sigma_{\theta 1} = \frac{T_{\theta\theta}}{Y_1} = \frac{\Omega_i R^{Ck+C-1} r_2^{Ck-t-6} (Ck+C+k) (1 + R_0^{t+k+1} r_2^{-2}) E_\theta \nu_{r\theta}}{R_0^{Ck} [R_0^{Ck+C+k} (E_\theta \nu_{r\theta} - E_\theta) + 1]},$$

$$\sigma_{r1} = \frac{T_{rr}}{Y_1} = \frac{r_2^{2Ck+2C-t-5} R^{Ck+C-1} \Omega_i R_0^C (1 + R_0^{t+k+1} r_2^{-2}) E_\theta \nu_{r\theta}}{R_0^{Ck+C+k} (E_\theta \nu_{r\theta} - E_\theta) + 1} + \frac{\Omega_i (1 - R^{t+k+3})}{R^{k+1} (t+k+3)} - \frac{\Omega_i r_2^{2Ck+2C+k-t-5} (1 + R_0^{t+k+1} r_2^{-2}) E_\theta \nu_{r\theta} R_0^k}{R^k [R_0^{Ck+C+k} (E_\theta \nu_{r\theta} - E_\theta) + 1]},$$

$$u = r_2 R \left[\frac{\Omega_i R_0^C R^{Ck+C-1} r_2^{2Ck+3C-t-8} (Ck+C+k)(1+R_0^{t+k+1} r_2^{-2}) E_\theta v_{r\theta}}{[R_0^{Ck+C+k} (E_\theta v_{r\theta} - E_r) + 1] E_\theta} - \frac{v_{r\theta}}{E_r} \left\{ \frac{r_2^{2Ck+2C-t-5} R^{Ck+C-1} \Omega_i R_0^C (1+R_0^{t+k+1} r_2^{-2}) E_\theta v_{r\theta}}{R_0^{Ck+C+k} (E_\theta v_{r\theta} - E_\theta) + 1} + \frac{\Omega_i (1-R^{t+k+3})}{R^{k+1} (t+k+3)} - \frac{\Omega_i r_2^{2Ck+2C+k-t-5} (1+R_0^{t+k+1} r_2^{-2}) E_\theta v_{r\theta} R_0^k}{R^k [R_0^{Ck+C+k} (E_\theta v_{r\theta} - E_\theta) + 1]} \right\} \right] \tag{19}$$

For fully plastic state, $C_{11} = C_{12} = C_{13}$, $C_{21} = C_{22} = C_{23}$, $C_{31} = C_{32} = C_{33}$, $C = C_{21}/C_{11} = C_{22}/C_{11} = C_1$. (20)

From Eqs. (19) and (20), stresses, angular velocity, and displacement in fully plastic state are $\frac{\rho_0 \omega^2 r_2^2}{\gamma} = \Omega_i =$

$$\left. \begin{aligned} & \frac{E_r v_{r\theta} [R_0^{C_1k+C_1+k} (E_\theta v_{r\theta} - E_\theta) + 1] R_0^{2k+1} (t+k+3) R_0^{C_1k+C_1+3k+3t+4}}{(1+R_0^{t+k+1} r_2^{-2}) E_\theta v_{r\theta} r_2^{t+2k+1} R_0^{2k+1} (t+k+3) + (r_2^{k+1} + R_0^{t+1} r_2^{t+1}) [R_0^{Ck+C+k} (E_\theta v_{r\theta} - E_\theta) + 1] [R_0^{C_1k+C_1+k-1} r_2^{-1} - R_0^{-k-1} r_2^{-k-1} - (C_1k+C_1+k) R_0^{C_1-1} r_2^{C_1-1}]} \\ \sigma_{\theta 1} = \frac{T_{\theta\theta}}{Y_1} &= \frac{\Omega_i R^{C_1k+C_1-1} r_2^{C_1k-t-6} (C_1k+C_1+k)(1+R_0^{t+k+1} r_2^{-2}) E_\theta v_{r\theta}}{R_0^{C_1k} [R_0^{C_1k+C_1+k} (E_\theta v_{r\theta} - E_\theta) + 1]} \\ \sigma_{r1} = \frac{T_{rr}}{Y_1} &= \frac{r_2^{2C_1k+2C_1-t-5} R^{C_1k+C_1-1} \Omega_i R_0^{C_1} (1+R_0^{t+k+1} r_2^{-2}) E_\theta v_{r\theta}}{R_0^{C_1k+C_1+k} (E_\theta v_{r\theta} - E_\theta) + 1} + \frac{\Omega_i (1-R^{t+k+3})}{R^{k+1} (t+k+3)} - \frac{\Omega_i r_2^{2C_1k+2C_1+k-t-5} (1+R_0^{t+k+1} r_2^{-2}) E_r v_{r\theta} R_0^k}{R^k [R_0^{C_1k+C_1+k} (E_\theta v_{r\theta} - E_\theta) + 1]} \\ u = r_2 R & \left[\frac{\Omega_i R_0^{C_1} R^{C_1k+C_1-1} r_2^{2C_1k+3C_1-t-8} (C_1k+C_1+k)(1+R_0^{t+k+1} r_2^{-2}) E_\theta v_{r\theta}}{[R_0^{C_1k+C_1+k} (E_\theta v_{r\theta} - E_\theta) + 1] E_\theta} - \frac{v_{r\theta}}{E_r} \left\{ \frac{r_2^{2C_1k+2C_1-t-5} R^{C_1k+C_1-1} \Omega_i R_0^{C_1} (1+R_0^{t+k+1} r_2^{-2}) E_\theta v_{r\theta}}{R_0^{C_1k+C_1+k} (E_\theta v_{r\theta} - E_\theta) + 1} + \frac{\Omega_i (1-R^{t+k+3})}{R^{k+1} (t+k+3)} - \frac{\Omega_i r_2^{2C_1k+2C_1+k-t-5} (1+R_0^{t+k+1} r_2^{-2}) E_\theta v_{r\theta} R_0^k}{R^k [R_0^{C_1k+C_1+k} (E_\theta v_{r\theta} - E_\theta) + 1]} \right\} \right] \end{aligned} \right. \tag{21}$$

NUMERICAL DISCUSSIONS

From Eqs.(22)-(24) and values of material constants given in Table 1, we get the values of modulus of elasticity and Poisson’s ratio for the considered materials, Table 2.

Stress strain relation for a plane stress condition,

$$\begin{bmatrix} e_{rr} \\ e_{\theta\theta} \\ e_{r\theta} \end{bmatrix} = \begin{bmatrix} \frac{1}{E_r} & -\frac{\nu_{r\theta}}{E_\theta} & 0 \\ -\frac{\nu_{r\theta}}{E_r} & \frac{1}{E_\theta} & 0 \\ 0 & 0 & \frac{1}{G_{r\theta}} \end{bmatrix} \begin{bmatrix} T_{rr} \\ T_{\theta\theta} \\ T_{r\theta} \end{bmatrix} \tag{22}$$

Stiffness matrix for orthotropic materials,

$$\begin{bmatrix} e_{rr} \\ e_{\theta\theta} \\ e_{zz} \end{bmatrix} = \begin{bmatrix} S_{11} & S_{12} & S_{13} \\ S_{21} & S_{22} & S_{23} \\ S_{31} & S_{32} & S_{33} \end{bmatrix} \begin{bmatrix} T_{rr} \\ T_{\theta\theta} \\ T_{zz} \end{bmatrix}, \quad \begin{bmatrix} T_{rr} \\ T_{\theta\theta} \\ T_{zz} \end{bmatrix} = \begin{bmatrix} C_{11} & C_{12} & C_{13} \\ C_{21} & C_{22} & C_{23} \\ C_{31} & C_{32} & C_{33} \end{bmatrix} \begin{bmatrix} e_{rr} \\ e_{\theta\theta} \\ e_{zz} \end{bmatrix} \tag{23}$$

$$S = C^{-1} \tag{24}$$

Table 1. Material constants for isotropic and orthotropic materials.

Materials (in 10 ¹⁰ Pa)	C11	C12	C13	C21	C22	C23
steel (isotropic material)	53.26	36.88	36.88	36.88	53.26	36.88
topaz (transversely isotropic)	28.145	12.552	8.433	12.552	34.911	8.825
barite (transversely isotropic)	8.941	4.614	2.691	4.614	7.842	2.676

Table 2. Modulus of elasticity and Poisson’s ratio for used materials.

Materials	E _r	E _θ	ν _{rθ}
steel (isotropic material)	27.7	27.7	0.69
topaz (transversely isotropic)	25	33.33	0.6
barite (transversely isotropic)	6.23	5.46	0.59

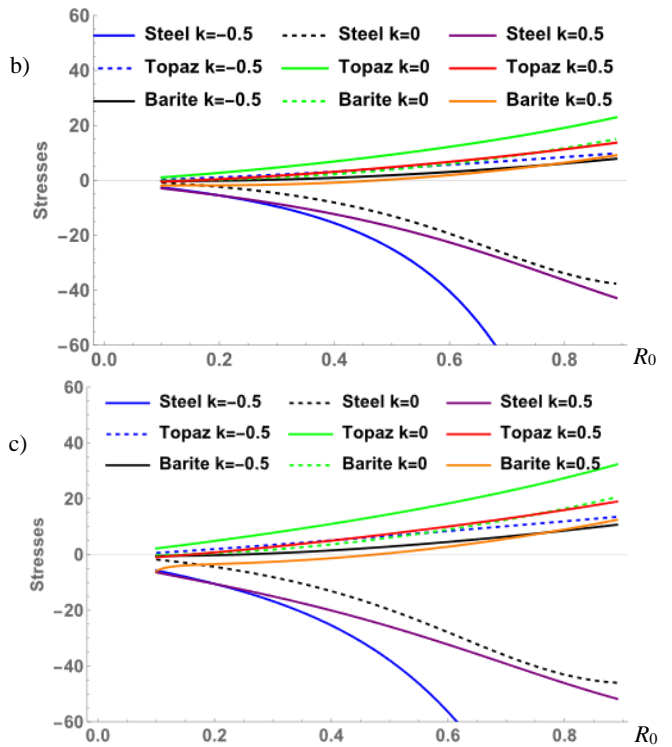
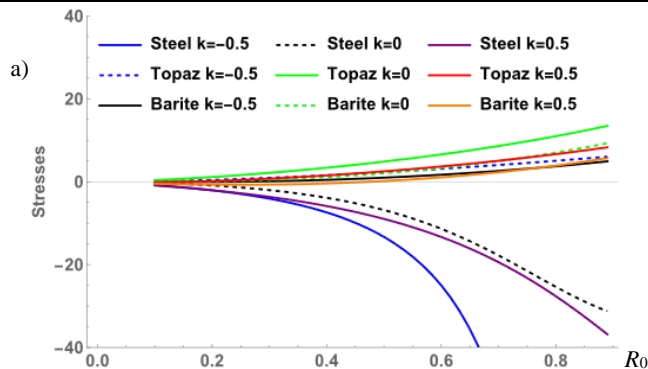


Figure 2. Angular velocity in elastic state for density parameter $t = 0, 0.3, 0.5$.

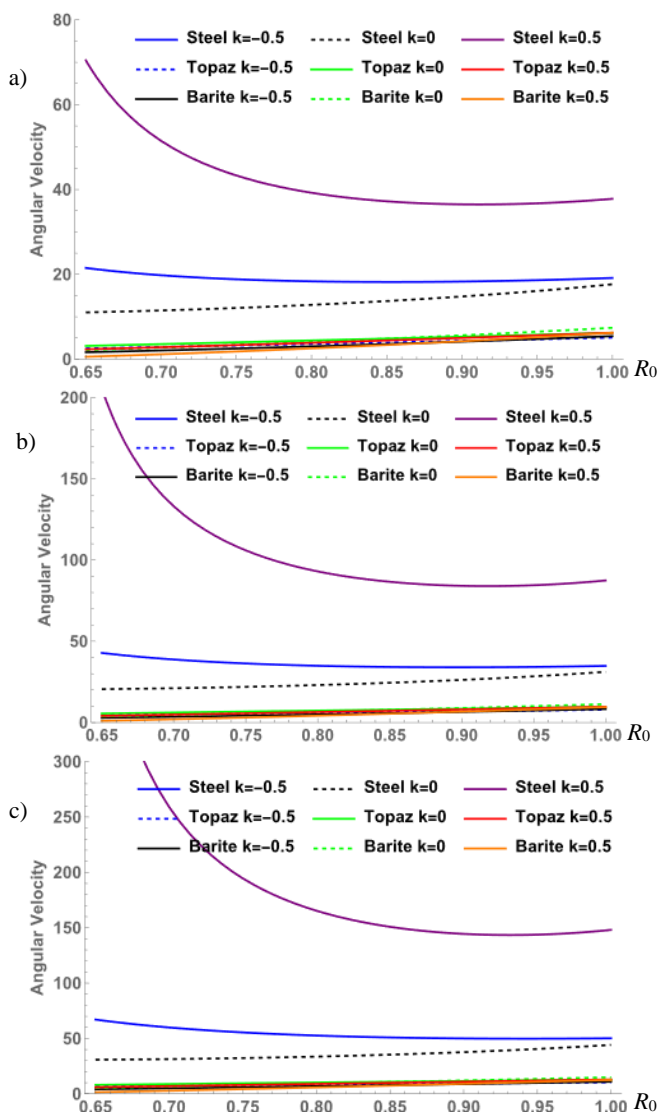


Figure 3. Angular velocity; plastic state; density param. $t = 0, 0.3, 0.5$.

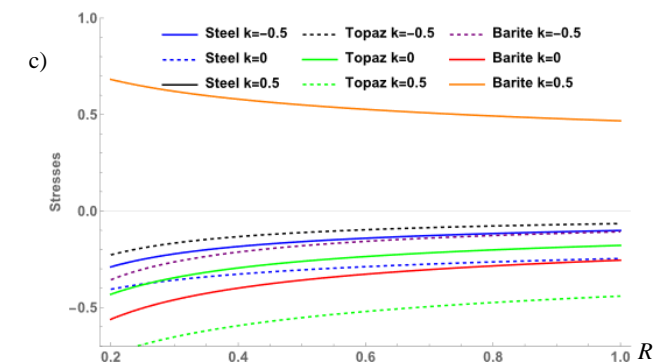
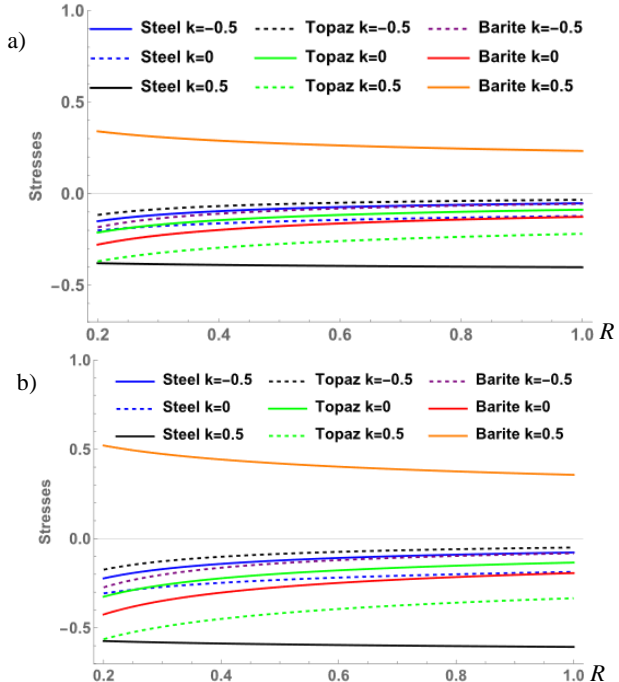


Figure 4. Circumf. Stresses; elastic state; density param. $t = 0, 0.3, 0.5$.

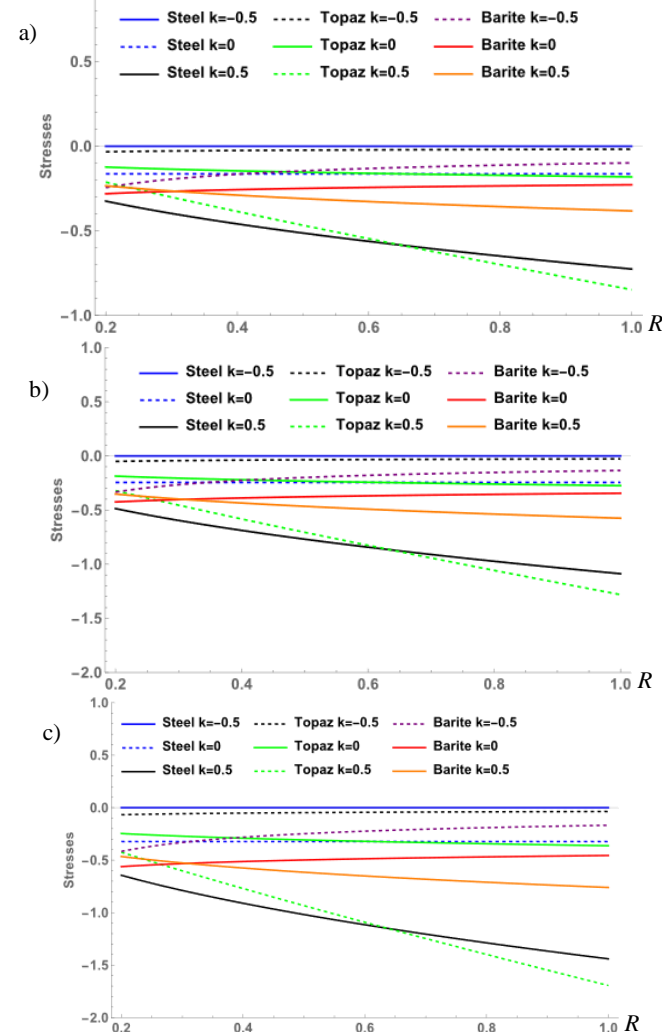
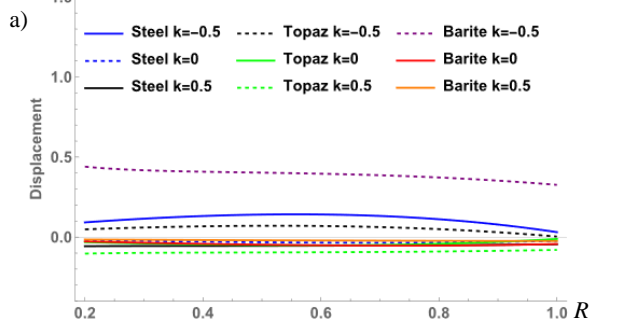


Figure 5. Circumf. Stresses; plastic state; density param. $t = 0, 0.3, 0.5$.



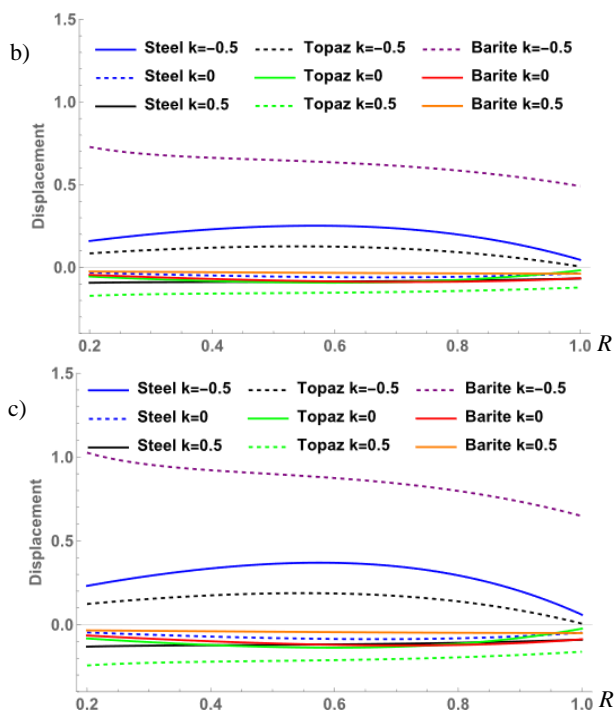


Figure 6. Displacement; elastic state; density param. $t = 0, 0.3, 0.5$.

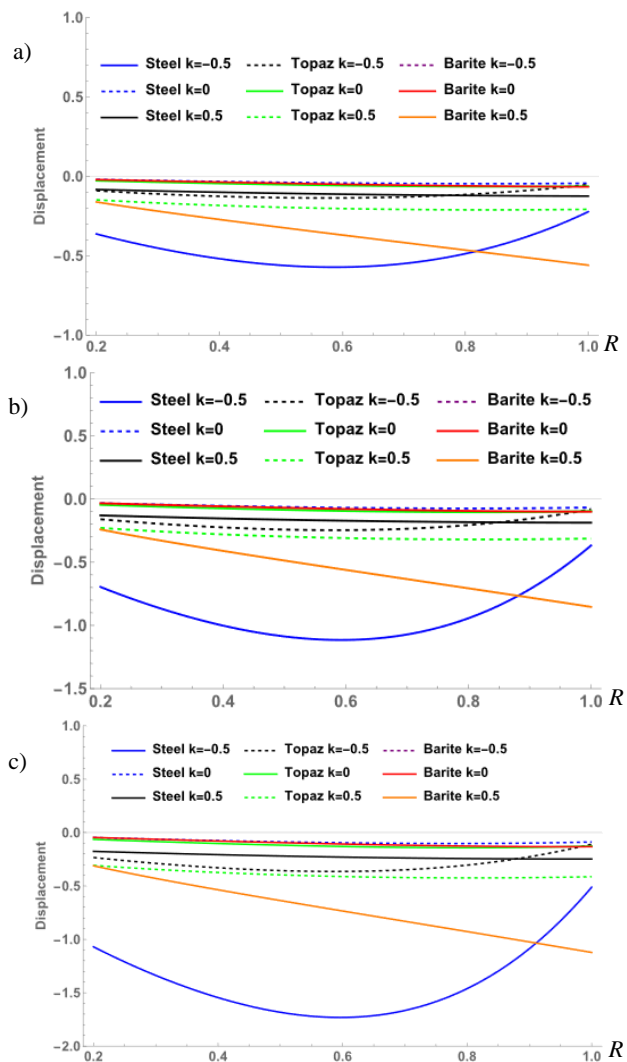


Figure 7. Displacement; plastic state; density param. $t = 0, 0.3, 0.5$.

NUMERICAL DISCUSSION AND CONCLUSION

To determine the stress distribution, displacement, and angular velocity for the hyperbolic rotating disc composed of isotropic (steel) and orthotropic material (topaz and barite), the Figs. 1-6 are drawn. The following numerical values are used in calculations: radii ratios $R = (r/r_2)(0.2 - 1.0)$; $k < 0$ (let -0.5 for convergent disc); $k > 0$ (let 0.5 for divergent disc); $k = 0$ (for uniform disc). Values of material constants, modulus of elasticity, and Poisson's ratio are taken from the Tables 1 and 2. Graphs are drawn for angular speed with different radii ratios in elastic and in plastic state with and without density parameter ($t = 0, 0.3, 0.5$) as presented in Fig. 2. It can be seen from Fig. 2a that the convergent disc composed of orthotropic material (topaz) needs higher angular velocity for initial yielding at inner surface of the disc as compared to isotropic material steel and orthotropic material barite. Also, angular velocity increases with radii ratio and attains its highest value at the outer surface of the disc for all considered materials. The addition of density parameter causes the angular velocity to increase as shown in Figs. 2b and 2c. Figure 3 shows the graphs of the angular velocity in fully plastic state with density parameter $t = 0, 0.3, 0.5$. It is observed that angular velocity is maximal in the case of the convergent disc of isotropic material steel as compared to other considered materials. In case of the uniform and divergent disc, the angular velocity is again higher in the topaz disc at initial yielding stage, but in the fully plastic stage the angular velocity is high in case of uniform steel disc and divergent topaz. Values of angular velocity rise as density parameter increases in case of both uniform and divergent discs, as can be seen in Figs. 3b and 3c.

Figures 4 and 5 show graphs of circumferential stresses in elastic and plastic states, respectively, for uniform, convergent, and divergent discs with different thickness parameters.

It is shown that stresses are of compressible nature for both isotropic and orthotropic materials. These stresses are higher in the convergent disc of topaz as compared to other materials in the elastic state, as seen in Fig. 4a. From Figs. 4b and 4c it is observed that stresses significantly increase with the addition of the thickness parameter. In this case the divergent disc stresses are maximal when made of barite (orthotropic material) in comparison to steel and topaz. For the uniform disc, stresses are again maximal when made of topaz. From Fig. 5, it is observed that in the plastic state, the stresses are tensile and show the same behaviour as in the elastic state. Elastic state stresses are highest for convergent disc of topaz and these stresses are the highest for uniform disc of barite and divergent topaz disc. Also, circumferential stresses show increase with thickness parameter ($t = 0.3, 0.5$).

Figures 6 and 7 are drawn to identify the behaviour of displacement with different radii ratios and thickness parameters in elastic and plastic states. Figure 6 shows that for divergent, uniform, and convergent discs, the displacement is largest near the disc's outer surface. In addition, compared to steel and topaz, the displacement is largest in the convergent disc of orthotropic material (barite). Figures 6b and 6c further demonstrate how displacement values rise as the thickness parameter increases. Figure 7 shows the variation

of displacement with various radii ratios in plastic state. It is observed that displacement is maximal at the outer surface of the disc, also in the case the disc is of isotropic material (steel), the displacement is the greatest. With increase in thickness parameter, the displacement also increases.

CONCLUSION

Elastic-plastic stresses are evaluated analytically by applying transition theory in a hyperbolic rotating disc with variable thickness composed of orthotropic material. In order to identify the variation of angular velocity, stresses, and displacement with radii ratios, the discs of isotropic (steel) and orthotropic materials (topaz and barite) are considered. Based on all the data and quantitative computations, the ensuing deductions are drawn.

Angular velocity is maximum in the convergent disc made of topaz (orthotropic) in elastic state, but in the plastic state, the angular velocity is maximum for divergent disc of steel.

Stresses in the elastic state are highest in divergent disc made of barite as compared to other considered materials. Fully plastic stresses are compressive and highest in the divergent disc made of topaz at the outer surface.

Displacement has the highest value at the outer surface for the convergent disc of steel.

Depending on all the observations and discussions it is deduced that the convergent disc made of topaz can be considered as favourable for engineering design purposes.

REFERENCES

- Sokolnikoff, I.S., *Mathematical Theory of Elasticity*, 2nd Ed., McGraw-Hill Inc., New York, 1953.
- Swainger, K.H., *Analysis of Deformation*, Chapman & Hall, London; Macmillan, USA, Vol.III, Fluidity, 1956, pp.67-68.
- Seth, B.R. (1962), *Transition theory of elastic-plastic deformation, creep and relaxation*, Nature, 195: 896-897. doi: 10.1038/195896a0
- Seth, B.R. (1966), *Measure-concept in mechanics*, Int. J Non-Linear Mech. 1(1): 35-40. doi: 10.1016/0020-7462(66)90016-3
- Timoshenko, S.P., Goodier, J.N., *Theory of Elasticity*, Third Ed., Mc Graw-Hill Book Co. New York, London, 1951.
- Sharifi, H. (2022), *Generalized coupled thermoelasticity in an orthotropic rotating disk subjected to thermal shock*, J Therm. Stress. 45(9): 695-719. doi: 10.1080/01495739.2022.2091066
- Matvienko, O., Daneyko, O., Valikhov, V., et al. (2023), *Elastoplastic deformation of rotating disk made of aluminum dispersion-hardened alloys*, Metals. 13(6): 1028. doi: 10.3390/met13061028
- Bayat, S.H., Nazari, M.B. (2023), *Dynamic crack analysis in anisotropic media under wave-like thermal loading*, Europ. J Mech. - A/Solids, 99: 104913. doi: 10.1016/j.euromechsol.2023.104913
- Zanchini, M., Longhi, D., Mantovani, S., et al. (2023), *Fatigue and failure analysis of aluminium and composite automotive wheel rims: Experimental and numerical investigation*, Eng. Fail. Anal. 146: 107064. doi: 10.1016/j.engfailanal.2023.107064
- Verma, G., Thakur, P. (2022), *Comparative creep analysis of spherical shell made up of different materials*, Mech. Solids, 57(5): 1214-1221. doi: 10.3103/S0025654422050120
- Temesgen, G.A., Singh, S.B., Pankaj, T. (2022), *Modeling of creep deformation in an internally pressurized transversely isotropic spherical shell subjected to a thermal gradient*, Mech. Solids, 57(4): 937-948. doi: 10.3103/S0025654422040185
- Thakur, P., Sethi, M., Gupta, N., Gupta, K. (2021), *Thermal effects in rectangular plate made of rubber, copper and glass materials*, J Rubber Res. 24: 147-155. doi: 10.1007/S42464-020-00080-6 (2021)
- Salehian, M., Shahriari, B., Yousefi M. (2019), *Investigating the effect of angular acceleration of the rotating disk having variable thickness and density function on shear stress and tangential displacement*, J Braz. Soc. Mech. Sci. Eng. 41: 31. doi: 10.1007/s40430-018-1523-8
- Singh, R., Saxena, R.K., Khanna, K., Gupta, V.K. (2020), *Creep response of rotating composite discs having exponential hyperbolic linear and constant thickness profiles*, Defence Sci. J, 70 (3): 292-298. doi: 10.14429/dsj.70.14913
- Lin, W.F. (2020), *Elastic analysis for rotating functionally graded annular disk with exponentially-varying profile and properties*, Math. Probl. Eng. 2020(1): Art. ID 2165804 doi: 10.1155/2020/2165804
- Jalali, M.H., Shahriari, B. (2018), *Elastic stress analysis of rotating functionally graded annular disk of variable thickness using finite difference method*, Math. Probl. Eng. 2018: Art. ID 1871674. doi: 10.1155/2018/1871674
- Yıldırım, V. (2018), *Closed-form formulas for hyperbolically tapered rotating disks made of traditional materials under combined thermal and mechanical loads*, Int. J Eng. Appl. Sci. 10 (2): 73-92. doi: 10.24107/ijeas.443239
- Sharma, R. (2023), *Evaluation of thermal elastic-plastic stresses in transversely isotropic disk made of piezoelectric material with variable thickness and variable density subjected to internal pressure*, Struct. Integr. Life, 23(2): 205-212.
- Matvienko, O., Daneyko, O., Valikhov, V., et al. (2023), *Elastoplastic deformation of rotating disk made of aluminum dispersion-hardened alloys*, Metals, 13(6): 1028. doi: 10.3390/met13061028
- Es-Saheb, M.H., Fouad, Y. (2023), *Creep analysis of rotating thick cylinders subjected to external and internal pressure: analytical and numerical approach*, Appl. Sci. 13(21): 11652. doi: 10.3390/app132111652
- Thakur, P., Sethi, M., Kumar, N., et al. (2022), *Stress analysis in an isotropic hyperbolic rotating disk fitted with rigid shaft*, Z. Angew. Math. Phys. 73: 23. doi: 10.1007/s00033-021-01663-y

© 2024 The Author. Structural Integrity and Life, Published by DIVK (The Society for Structural Integrity and Life 'Prof. Dr Stojan Sedmak') (<http://divk.inovacionicentar.rs/ivk/home.html>). This is an open access article distributed under the terms and conditions of the Creative Commons Attribution-NonCommercial-NoDerivatives 4.0 International License